Highly Efficient Debromination of 4,4′-dibrominated Diphenyl Ether by Organic-palygorskite Supported Pd/Fe Nanoparticles

Jiang Shao
Yancheng Teachers University
Yi Zhang
Yancheng Teachers University
Zongtang Liu (zongtliu@163.com)
Yancheng Teachers University
Zhenghao Fei
Yancheng Teachers University
Yufeng Sun
Yancheng Teachers University
Ziyan Chen
Yancheng Teachers University
Xiaoju Wen
Yancheng Teachers University
Weizhong Shi
Yancheng Teachers University
Dandan Wang
Yancheng Institute of Technology
Chenggang Gu
CAS Institute of Soil Science: Institute of Soil Science Chinese Academy of Sciences

Research Article

Keywords: Nanoscale zerovalent Pd/Fe particles, organic-palygorskite, PBDEs, debromination, mechanism

Posted Date: July 28th, 2021

DOI: https://doi.org/10.21203/rs.3.rs-667512/v1

Version of Record: A version of this preprint was published at Environmental Science and Pollution Research on August 18th, 2021. See the published version at https://doi.org/10.1007/s11356-021-15997-7.

Abstract

Organic-palygorskite (OP) supported Pd/Fe nanoparticles composite (OP-Pd/Fe) was prepared by stepwise reduction method. The removal capacity of 4,4′-dibrominated diphenyl ether (BDE15) by OP-Pd/Fe was compared with other various materials. For better understanding the possible mechanism, the synthesized and reacted OP-Pd/Fe materials were characterized by TEM, SEM, XRD, and XPS, respectively. The effects of major influencing parameters on the degradation of BDE15 were also studied. Benefit from the synergistic effect of the carrier and bimetallic nanoparticles, BDE15 could be completely debrominated into diphenyl ether (DE) under suitable conditions. A two-stage adsorption/debromination removal mechanism was proposed. The degradation of BDE15 with OP-Pd/Fe was mainly stepwise debromination reaction, and hydrogen transfer mode was assumed as the dominated debromination mechanism. The removal process fitted well to the pseudo first-order kinetic equation. The observed rate constants increased with increasing Pd loading and OP-Pd/Fe dosage, while decreased with increasing initial BDE15 concentration, the tetrahydrofuran/water ratio, and the initial pH of the solution. The work provides a new approach for the treatment of PBDEs pollution.

Introduction

As a group of nonreactive brominated flame retardant (BFR) chemicals, polybrominated diphenyl ethers (PBDEs) have been widely added to various commercial products in the past decades (Wong et al. 2012; Labunska et al. 2013). Because of their high persistence, easy bioaccumulation, and potential toxicity, tetra- to hepta-BDE congeners and deca-BDE have been added to the list of persistent organic pollutants (POPs) under the Stockholm Convention in 2009 and 2019, respectively (Zhu et al. 2014; Tan et al. 2017; Li et al. 2019; Wei et al. 2020a; Sarkar and Singh 2021). Although, PBDEs have been banned or phased out in Europe, Canada, and the U.S. market, deca-BDE is still the main commercial product in some Asian countries. PBDE congeners have been extensively detected in various environmental media and pose high risks to humans (Wurl et al. 2006; Muresan et al. 2010; Qin et al. 2011; Cheng and Ko 2018; Chen et al. 2020a). Especially, the lower-brominated PBDEs have stronger bioaccumulation, biotoxicity, and more resistance to natural biodegradation, should be given more attention (Ni et al. 2012; Labunska et al. 2013; Chen et al. 2020a; Lei et al. 2020). Therefore, effective and feasible reductive methods for removing low brominated PBDEs quickly and completely should be developed.

Nanoscale zerovalent iron (nZVI) materials have been widely applied to remove halogenated organic pollutants due to its high reactivity and great degradation efficiency (Doong and Lai 2006; Kim et al. 2008; Zhuang et al. 2010; Wang et al. 2011; Xie et al. 2014). However, nZVI is easily oxidized and agglomerated, which can result in a decrease of the degradation performance. Previous studies indicated that using various supporting material or adding a second metal to increase the dispersity and stability of nZVI was a promising approach to deal with these problems (Zhuang et al. 2011; Zhang et al. 2015; Shen et al. 2017; Tan et al. 2017; Hou et al. 2020). Clay minerals as abundant natural resources are widely used as the supporting materials due to their good dispersion for nZVI and adsorption capacity for contaminants, thus can enhance the efficiency of nZVI (Weng et al. 2014b; Liu et al. 2015; Zhang et al.

2015; Ezzatahmadi et al. 2017). Although clay minerals can reduce the aggregation of nZVI and increase its stability, the low reductive ability still hinders its further dehalogenation application. In order to improve the reactivity for reductive dehalogenation, many second metals like Ag, Cu, Pd, and Ni have been loaded on the nZVI surface to prepare various Fe-based bimetallic nanoparticles (Duan et al. 2016; Wang et al. 2019; Xu et al. 2020). Among these bimetallic nanoparticles, Pd/Fe nanoparticles exhibit much higher reactivity (Wang et al. 2019). The clay minerals commonly used for water treatment are divided into 2:1 and 1:1 structural groups (Ezzatahmadi et al. 2017). Palygorskite (PAL) is one type of clays composed of ribbons with specifically alternating layers, has high specific surface area and surface groups (Guo et al. 2020). These properties are beneficial for PAL to be a catalyst support (Chen et al. 2020b). Nevertheless, natural PAL usually has poor adsorption capacity for organic pollutants which is unfavorable for the mass transfer. Accordingly, the organic modification of PAL by appropriate method is a viable way to improve its adsorption capacity and promote its using as an effective support material.

In this study, firstly, PAL was modified with octadecyl trimethylammonium chloride (OTAC) by ultrasonic treatment to obtain organic-PAL (OP). Then OP was used as the supporting material to prepare nZVI on OP (OP-Fe) by liquid-phase reduction. After that, OP-supported Pd/Fe nanoparticles (OP-Pd/Fe) composite was prepared by a simple impregnation-chemical reduction method. The resultant OP-Pd/Fe composite was then used as catalyst for the reductive debromination of 4,4′-dibrominated diphenyl ether (BDE15), which was one kind of typical low brominated PBDEs with strong resistance to degradation (Guo et al. 2019). Here, OP was considered as both adsorbent and support of Pd/Fe nanoparticles, Fe acted as an electron source, while the Pd nanoparticles provided localized catalytic sites. The OTA^+ in OP carrier could stabilize highly dispersed Pd/Fe nanoparticles and protect them from oxidation. The overall objectives of this research were to: 1) find out the function of support and bimetallic nanoparticles; 2) identify the possible reaction mechanism; 3) test the major influencing parameters (Pd loading, dosage of OP-Pd/Fe, initial BDE15 concentration, solvent condition, and pH; and 4) discuss the degradation kinetics of BDE15 with OP-Pd/Fe.

Materials And Methods

Materials and chemicals

BDE15 (>98%) and 4-brominated diphenyl ether (BDE3, >99%) were supplied by Chem Service, Inc. Diphenyl ether (DE) (>99.5%) was purchased from the Aladdin Reagent Co., Ltd. HPLC grade tetrahydrofuran (THF) and methanol were obtained from J&K Scientific Ltd. Ferrous sulfate ($FeSO_4·7H_2O$, >99%), potassium tetrachloropalladate (K_2PdCl_4, >99%), sodium borohydride ($NaBH_4$, >98%), and OTAC were acquired from Sinopharm Chemical Reagent Co., Ltd. PAL was purchased from Zhongcai attapulgite Clay Co., Ltd.

Preparation and characterization of the materials

OP was prepared by modifying PAL with OTAC (OTA^+ was 11.6 weight % of PAL) according to previous studies (Huang et al. 2007; Liu et al. 2014). OP-Pd/Fe was synthesized via the liquid-phase reduction method where OP acted as a supporting material according to previous report (Ezzatahmadi et al. 2017). 2.50 g $FeSO_4 \cdot 7H_2O$ was dissolved by 100 mL of mixture solution (absolute ethanol and distilled water at a volume ratio of 2:3) in a four-neck flask, and then added OP (the mass ratio of OP:Fe was 2:1). The mixture was agitated with a mechanical mixer for 30 min under nitrogen atmosphere, and then 1.0 mol/L $NaBH_4$ solution (50 mL) was added into the mixture drop by drop to cause the liquid phase reduction. Subsequently, the mixture was stirred continuously under nitrogen atmosphere for another 30 min. The composite (OP-Fe) was obtained by vacuum filtration, and rapidly washed with deoxygenated absolute ethanol three times. The freshed OP-Fe was added into a four-neck flask with 50 mL of K_2PdCl_4 solution to deposit enough elemental palladium on the zerovalent iron particles (the Pd loading ranged from 0.025% wt_{Fe} to 0.2% wt_{Fe}). The mixture was continued stirring under nitrogen atmosphere for 30 min to ensure the palladium was completely deposited on the iron surface by the redox reaction. The OP-Pd/Fe composite was rinsed with deoxygenated distilled water and absolute ethanol for three times in turn, then vacuumly dried at 333 K for 12 h. Nanoscale zerovalent iron (nZVI) and Pd/Fe bimetallic particles without adding OP, and PAL supported Pd/Fe composite were also prepared using the same method.

The morphology and particle size of materials were analyzed using scanning electron microscopy (SEM, JEOL JSM-5610LV, Japan) and transmission electron microscopy (TEM, JEOL-2100F, Japan), respectively. X-ray diffraction (XRD) patterns were acquired by an X-ray diffractometer (Rigaku ULTIMA IV, Japan) at 40 kV/40 mA. A high-power Cu Kα radiation source (0.154 nm) was applied in the X-ray experiments. X-ray photoelectron spectroscopic (XPS) analysis was conducted on a Thermo Scientific K-Alpha$^+$ spectrometer (Thermo Electron Corporation, USA). Al Kα radiation was used as the exciting source (72 W). The actual values of Pd loading were detected by ICP-OES (Perkin Elmer OPTIMA 8000DV, USA).

Batch experiments

The removal of BDE15 experiment was conducted in 250 mL conical flask with cover, where OP-Pd/Fe was added into 100 mL BDE15 tetrahydrofuran/water (THF/W) mixed solution (THF was used to enhance BDE15 solubility). Then the conical flask was oscillated at 150 rpm and the temperature was controlled at 25 ± 1 °C. 0.5 mL suspension was removed from the conical flask at fixed time intervals and filtered through the 0.22μm filter membrane. The concentrations of BDE15 and its degradation products (BDE3 and DE) were analyzed by HPLC system (Waters e2695, USA) equipped with a UV detector and a Waters C18 column (5 μm×250 mm×4.6 mm). The mobile phase was 90% methanol and 10% water at 1.0 mL/min. The λ of UV detector was set at 240 nm, and the column temperature was 30 ± 1 °C. All removal experiments were conducted in triplicate. The degradation kinetics was described in Supporting Information (Section S1).

Removal experiments of BDE15 using supporting material and other Fe-based nanoparticles were conducted as same as that of OP-Pd/Fe. Major influencing parameters, Pd loading (0.025%, 0.05%, 0.1%,

and 0.2% wt_{Fe}), OP-Pd/Fe dosage (0.5, 1.0, 2.0, and 3.0 g/L), initial BDE15 concentration (5, 10, 15, 20, and 25 mg/L), THF/W ratios (30/70, 40/60, 50/50, 60/40, and 70/30), and solution pH (2.2, 3.0, 5.0, 7.0, 9.0, and 11.0, which was adjusted by 0.5 mol/L H_2SO_4 or 1.0 mol/L NaOH) were investigated. Except the investigated parameter, other parameters fixed on Pd loading 0.05% wt_{Fe}, 3.0 g/L OP-Pd/Fe, 10 mg/L BDE15, THF/W = 50/50, and pH = 7.0.

Results And Discussion

Removal of BDE15 by various materials

To understand the difference between the removal of BDE15 by support and various Fe-based nanoparticles, experiments were conducted as depicted in Fig. 1. The dosages of OP, OP-Fe, OP-Pd/Fe, and PAL-Pd/Fe were 3.0 g/L, while the dosages of nZVI and Pd/Fe reduced to 1.0 g/L to keep the same Fe mass in the reaction system. When using OP as control, the removal efficiency of BDE15 only arrived at 9.3% during 360 min reaction, which was due to the adsorption of the supporting material OP for BDE15. The removal efficiency of BDE15 by nZVI was 16.9% in 360 min which could be ascribed to the reductive ability of nZVI. The BDE15 removal efficiency of OP-Fe achieved 36.4% which was much higher than the sum (26.2%) of removal efficiency when using OP and nZVI alone. This was because the support OP was an efficient stabilizer to reduce the extent of nZVI aggregation and expose highly reactive particles directly to BDE15 (Ezzatahmadi et al. 2017).

From Fig. 1, it could also be seen that OP-Pd/Fe had excellent removal performance for BDE15 compared to OP-Fe, the removal efficiency arrived at 100% after 90 min reaction. This might be due to the outstanding degradation activity of Pd/Fe bimetallic particles. Previous studies indicated that Pd as a catalyst was in favour of nZVI corrosion and the formation of active hydrogen for debromination (Wang et al. 2013; Xu et al. 2013b; Wei et al. 2020b). To ascertain the effect of the OP for OP-Pd/Fe composite removal efficiency, unsupported Pd/Fe bimetalic nanoparticles and PAL-Pd/Fe were also used to reduce BDE15 under identical conditions. As illustrated in Fig. 1, the removal efficiency of BDE15 by Pd/Fe, OP-Pd/Fe, and PAL-Pd/Fe within 60 min was 100%, 92.6%, and 77.9%, respectively. Although OP-Pd/Fe had better removal efficiency than PAL-Pd/Fe due to its enhanced adsorption capacity, obviously, Pd/Fe showed impressive performace on BDE15 removal. The result implied that the supporting material OP did not enhance the removal efficiency directly which was different with previous studies (Wang et al. 2013; Weng et al. 2014a). That phenomenon might be due to that the rapid corrosion of unsupported Pd/Fe bimetalic nanoparticles could supply sufficient active hydrogen for 10 mg/L BDE15 debromination. However, according to previous studies, the aggregation of unsupported Pd/Fe nanoparticles could reduce their reactivity and stability (Smuleac et al. 2011; Xu et al. 2013a; Wang et al. 2014). The stability of OP-Pd/Fe (3.0 g/L) and Pd/Fe (1.0 g/L) was successively examined by adding BDE15 repeatedly into the reaction system. The time intervals were selected when BDE15 removal efficiency was more than 95% at the first removal cycle, and BDE15 was added into the system to reach the initial concentration of 10 mg/L according to the former detected results. As shown in Fig. 2a, OP-Pd/Fe exhibited only a slight loss of reactivity to BDE15 after four cycles. While, Pd/Fe showed an obvious loss of reactivity to BDE15 after

only two cycles (Fig. 2b). Although Pd/Fe had more large removal rate, OP-Pd/Fe possessed superior long-term stability with the BDE15 accomulative removal amount about 145.3 mg/g. This could be ascribed to the good dispersion of OP for Pd/Fe bimetallic particles to decrease the aggregation. Moreover, OP could adsorb Fe^{2+} formed by nZVI corrosion (Ezzatahmadi et al. 2017), and decrease formation of ferrous (hydro) oxides, which would precipitate on the Pd/Fe surface and inhibit the reaction (Wei et al. 2020b).

Characterization

The above removal results demonstrated the different removal efficiencies of various meterials. For better understanding the underlying removal mechanism, it is important to find out the structural information and surface morphology of various materials. The morphology of OP, Pd/Fe, OP-Pd/Fe before and after reaction was characterized by TEM and SEM, and the results were depicted in Fig. 3 and Fig. 4. Fig. 3a and Fig. 4a showed that OP had natural one-dimensional nanorod-like structure and small ravines appeared among different nanorods, which could offer high specific surface for nZVI loading (Liu et al. 2015). As displayed in Fig. 3b and Fig. 4b, the prepared Pd/Fe nanoparticles were assembled in chain like structures with the particle size of about 50–100 nm due to magnetic interaction. In contrast, Fig. 3c and Fig. 4c demonstrated that the Pd/Fe nanoparticles loaded on OP surface were better dispersed with an average particle diameter of 30–80 nm. The results indicated that an improved dispersion of Pd/Fe nanoparticles occurred because of the interaction between the Pd/Fe nanoparticles and OP material. Seen from Fig. 3d, after reacting with BDE15 for 360 min, the size of Pd/Fe nanoparticles on OP decreased significantly because of the reaction of Pd/Fe with BDE15 and corrosion of nZVI (Xie et al. 2021). Moreover, as shown in Fig. 3d and Fig. 4d, the surface of the OP-Pd/Fe after reaction became more irregular.

The XRD patterns of OP, OP-Pd/Fe before and after reaction with BDE15, and Pd/Fe before and after reaction with BDE15 were shown in Fig. 5. From Fig. 5a to 5c, it was found that there were obvious characteristic diffraction peaks of OP at 2θ = 8.35°, 16.29°, 19.82°, 20.77°, 26.68°, 27.73°, and 35.14°. The characteristic peaks at 2θ = 44.80° in OP-Pd/Fe and Pd/Fe before reaction in Fig. 5b and Fig. 5d were ascribed to Fe^0. But the characteristic peak of Pd^0 (40.00°) was not clearly detected attributed to Pd loading less than XRD detection limit (Lei et al. 2020; Wei et al. 2020b). As shown in Fig. 5c, after reacting with BDE15 for 360 min, the characteristic diffraction peak at 2θ = 44.80° of OP-Pd/Fe disappeared, while the peaks at 2θ = 30.22°, 35.60°, 43.29°, 57.24°, and 62.84° were detected and could be ascribed to Fe_2O_3 and Fe_3O_4, proving the formation of iron oxide layers during the reaction (Tan et al. 2017; Wei et al. 2020b). However, the characteristic diffraction peaks of Pd/Fe after reaction were different from OP-Pd/Fe after reaction. Seen from Fig. 5e, the characteristic peaks of Fe^0 also disappeared and the characteristic peaks of Fe_2O_3 and Fe_3O_4 appeared. There were additional peaks appeared at 2θ = 21.21°, 36.65°, 41.20°, and 52.23°, which could be ascribed to α-FeOOH (Mokete et al. 2020; Xian et al. 2021). The results indicated that formation of ferrous (hydro) oxides on OP-Pd/Fe surface had been decreased because of the adsorption of Fe^{2+} by OP.

XPS analysis of Fe 2p and Pd 3d of OP-Pd/Fe before and after reaction was displayed in Fig. 6. As described in Fig. 6a and Fig. 6b, the peaks emerged at the binding energies of 725.4 eV and 712.9 eV were considered as Fe $2p_{1/2}$ and Fe $2p_{3/2}$ of iron oxides, which could be assigned to Fe_2O_3 and Fe_3O_4 (Wang et al. 2014; Wu et al. 2014; Talpade et al. 2019; He et al. 2020). While the distinctive peak observed at 707.1 eV in the Fe $2p_{3/2}$ region confirmed the existence of Fe^0 in OP-Fe/Pd (Hou et al. 2020). Furthermore, a shoulder at 719.0 eV was found as a result of the overlap of the shake-up satellite of iron oxides ($2p_{3/2}$) and Fe^0 (Talpade et al. 2019). Compared by the relative areas of Fe $2p_{3/2}$ peaks, the relative atomic percentage of iron oxides in OP-Pd/Fe after reaction increased from 82.2% to 100%. It approved that the iron corrosion did happen in the catalytic reaction process, which was accordant with the experimental results of XRD. As presented in Fig. 6c and Fig. 6d, the peaks at 340.4 eV and 335.1 eV in both samples were originated from Pd $3d_{3/2}$ and Pd $3d_{5/2}$ of Pd^0 (Zhou et al. 2018). It was convinced that the metallic Pd existed in OP-Fe/Pd before and after reaction. And there were no obvious differences of the relative contributions of Pd in OP-Pd/Fe before and after reaction. Therefore, it was considered that the iron corrosion occurred in aqueous solution with the generation of hydrogen and Pd acted as catalyst was responsible for hydrogen dissociation into active atomic hydrogen.

Debrominatin mechanism for BDE15 by OP-Pd/Fe

To further understand the debromination mechanism of BDE15 by OP-Pd/Fe, HPLC analysis of BDE15 and its byproducts during 180 min was shown in Fig. S1. As depicted in Fig. S1, the peak at 8.03 min was BDE15, and its intensity continuously weakened as the reaction proceeded. Moreover, BDE3 and DE chromatographic peaks appeared at retention time of 6.62 min and 5.37 min, respectively.

Fig. 7 showed the molar fraction changes of BDE15 and its debromination products in OP-Pd/Fe and Pd/Fe system, respectively. As illustrated in Fig. 7a, the removal efficiency of BDE15 by OP-Pd/Fe was only 5.7% within the first 15 min, the sum of BDE3 and DE molar fraction was only 0.9%. Therefore, adsorption was the main removal mechanism of OP-Pd/Fe for BDE15 in the first 15 min. However, the molar fraction of BDE15 decreased sharply after 15 min, and BDE3 molar fraction could reach 46.4% after 30 min. After then, the molar fraction of BDE3 began to decrease and BDE3 could be completely debrominated into DE within 180 min. Hence, the removal mechanism of BDE15 by OP-Pd/Fe was mainly reductive debromination. As shown in Fig. 7b, BDE15 in Pd/Fe system could be completely debrominated into BDE3 and DE within 60 min, while BDE3 could not continue to be completely debrominated into DE. The final debromination products of BDE15 by Pd/Fe were different from OP-Pd/Fe. The underlying mechanism to explain this difference was that OP-Pd/Fe system, where Pd/Fe nanoparticles were well dispersed on OP, could slow down the nZVI corrosion rate and maintain the catalytic activity of Pd/Fe nanoparticles.

The possible removal mechanism of BDE15 by OP-Pd/Fe was shown in Fig. 8. Firstly, the BDE15 molecules in the solution were adsorbed on the OP-Pd/Fe surface. Then nZVI in OP-Pd/Fe reacted with water to generate hydrogen, simultaneously hydrogen converted to atomic H* by the excellent catalyst Pd^0 (Xu et al. 2013a; Wang et al. 2017), where the two bromines in BDE15 were successively replaced by

the atomic H*. As described in Fig. 8, the debromination pathway proceeded as following: BDE15 → BDE3 → DE. So, the degradation of BDE15 with OP-Pd/Fe was mainly stepwise debromination reaction, and hydrogen transfer mode was assumed as the dominated debromination mechanism, which was similar to previous studies (Liu et al. 2015; Wiltschka et al. 2020).

Effect of experimental parameters on the degradation of BDE15

Effect of Pd loading

Previous studies affirmed that the amount of the catalyst played significant role in enhancing the debromination (Fang et al. 2011a; Wang et al. 2017; Lei et al. 2020). Considering the increase of debromination efficiency and the decrease of treatment cost, the optimal Pd loading should be determined (Huang et al. 2013; Zahran et al. 2013). When the theoretical Pd loading was 0.025%, 0.05%, 0.1%, and 0.2% wt_{Fe}, the actual value detected by ICP-OES was 0.0245%, 0.0457%, 0.0903%, and 0.173% wt_{Fe}, respectively. The actual Pd loading efficiency by nZVI reduction could reach higher than 86.5%. The effect of Pd loading on the debromination of BDE15 was shown in Fig. 9a. When the Pd loading was adjusted from 0 to 0.025% wt_{Fe}, the debromination efficiency of BDE15 within 240 min increased significantly from 33% to 92%. The debrominaiton efficiency obviously continued increase when the Pd loading was beyond 0.05% wt_{Fe}. This was attributed to the effect of Pd nanoparticles. More Pd nanoparticles could provide more reactive sites for formation of active H* for BDE15 debromination (Lei et al. 2020). Although, increasing Pd loading from 0.05% wt_{Fe} to 0.2% wt_{Fe} could decrease the BDE15 complete degradation time from 90 min to 40 min, the treatment cost was also enhanced. Therefore, in this study, the appropriate Pd loading of 0.05% wt_{Fe} could achieve complete debromination of BDE15 and was used in the following experiments.

The degradation of BDE15 by OP-Pd/Fe observed here exhibited a two-stage first-order degradation kinetics which was composed of a adsorption period (first-stage) and a followed rapid debromination period (second-stage) as appeared in Fig. S2. The simulated results of the degradation of BDE15 by OP-Pd/Fe were listed in Table S1. As shown in Table S1, the k_{obs1} values of the adsorption of BDE15 onto OP-Pd/Fe surface were obviously smaller than k_{obs2} values of rapid degradation under the same conditions.

Fig. S2a illustrated the effect of Pd loading on the two-stage degradation kinetics. When no Pd loaded, k_{obs1} value was almost equal to k_{obs2} within 240 min. While the Pd loading rose from 0.025% wt_{Fe} to 0.2% wt_{Fe}, the k_{obs1} value increased from 0.0027 min^{-1} to 0.0549 min^{-1}, and the k_{obs2} value increased from 0.0122 min^{-1} to 0.1393 min^{-1}. The removal rate of the two stage was enhanced 19.3 and 10.4 times, respectively. The results indicated that the degradation rate of BDE15 was related to the mass of Pd loaded on OP-Pd/Fe (Huang et al. 2013).

Effect of OP-Pd/Fe dosage

Dosage of OP-Pd/Fe affecting the degradation efficiency of BDE15 was displayed in Fig. 9b. Increasing OP-Pd/Fe dosage from 0.5 g/L to 3.0 g/L, the degradation efficiency of BDE15 increased from 9.0% to 96.6% after 60 min. Obviously, the degradation efficiency of BDE15 increased with the increase of the dosage of OP-Pd/Fe. It was due to that the reactive surface areas and the number of active sites could be simultaneously increased with the increase of OP-Pd/Fe dosage (Huang et al. 2013; Li et al. 2015). However, the degradation degree was only enhanced slightly when the OP-Pd/Fe dosage increased to 4.0 g/L. It indicated that, at a constant initial BDE15 concentration, 3.0 g/L OP-Pd/Fe could provide sufficient reactive surface areas and available active sites for the degradation. Moreover, the overdose of OP-Pd/Fe would generate excess hydrogen, which could cover the OP-Pd/Fe surface and hinder the adsorption of BDE15 (Wei et al. 2020a). Thus, the optimum OP-Pd/Fe dosage was 3.0 g/L in this research. As shown in Fig. S2b and Table 1S, from 0.5 g/L to 4.0 g/L OP-Pd/Fe dosage, the first-stage was shortened and the k_{obs2} value increased significantly from 0.0066 min^{-1} to 0.0803 min^{-1}. It indicated that much higher OP-Pd/Fe dosage could enhance the debromination rate of BDE15.

Effect of initial BDE15 concentration

The initial BDE15 concentration effect was studied by varying it from 5 mg/L to 25 mg/L. All of the BDE 15 concentrations investigated here are relevant for the process understanding in this case study, but do not refer to environmental relevant concentrations. As shown in Fig. 9c, 100% of BDE15 was degraded at 5 mg/L within 60 min, and it was only 29.5% within 60 min at 25 mg/L, which implied that the degradation efficiency of BDE15 decreased significantly as the initial BDE15 concentration increased. Generally, the removal of BDE15 by OP-Pd/Fe was a heterogeneous reaction, including adsorption of BDE15 on the material surface and the subsequent debromination (Wang et al. 2019). Further increase of initial BDE15 concentration would result in competitive adsorption between BDE15 molecules when the OP-Pd/Fe dosage was fixed (Huang et al. 2013). This was unfavourable for subsequent reduction, leading to a decline in removal efficiency of BDE15. Fig. S2d also indicated that the k_{obs2} value decreased with the increasing initial BDE15 concentration. From Table 1S, increasing the initial BDE15 concentration from 5 mg/L to 25 mg/L, the k_{obs2} value decreased from 0.0819 min^{-1} to 0.0117 min^{-1}.

Influence of of solvent conditions

Due to the strong hydrophobicity of BDE15 (Bohm et al. 2016), a certain proportion of organic solvents is needed to prepare the high concentration aqueous solution. The effect of THF proportion in solution on BDE15 degradation was shown in Fig. 9d. The degradation efficiencies were 97.0%, 92.4%, and 57.2% after 30 min when the THF/W ratios were 30/70, 40/60, and 50/50, respectively. While the THF/W rose to 60/40 and 70/30, the degradation efficiencies were only about 1.1% and 0.2% within 30 min, respectively. The main reason was that the the hydrogen ion content in the solvent determined the formation of hydrogen, and the degradation process was catalytic hydrogenation. Low proportion of water in aqueous solution was unfavourable for the corrosion of nZVI to generate hydrogen (Fang et al. 2011b). Moreover, there was another possible reason for the phenomenon. The removal of BDE15 by OP-Pd/Fe was a two-stage adsorption/debromination mechanism. The adsorption process depended on hydrophobic

interactions between the BDE15 molecule and the solid phase surface (Bohm et al. 2016). When increasing percentage of THF in the liquid phase, the adsorption of BDE15 onto OP-Pd/Fe decreased, and would accordingly lead to reducing the degradation efficiency. As seen from Fig. S2d and Table 1S, when the THF percentage rose from 30% to 70%, the first-stage period prolonged from 10 min to 90 min due to the decrease of BDE15 adsorption amount onto OP-Pd/Fe. Moreover, the k_{obs2} value sharply decreased from 0.1521 min^{-1} to 0.0083 min^{-1}. In this study, to ensure that BDE15 with high concentration was completely dissolved in aqueous solution, 50% THF was introduce to the aqueous solution. However, in future environmental applications, the high ratio organic solvent addition still needs careful consideration.

Effect of solution pH

The effect of different solution pH on the degradation of BDE15 by OP-Pd/Fe was presented in Fig. 9e. The degradation efficiencies were 100%, 97.3%, 96.6%, 72.4%, and 45.1% within 60 min as the solution pH were 3.0, 5.0, 7.0, 9.0, and 11.0, respectively. Obviously, the degradation efficiency of BDE15 declined while the solution initial pH value increased from 3.0 to 11.0. This could be explained that the low solution pH value was in favour of the corrosion of nZVI (Weng et al. 2014b), including the generation of more H_2 and the formation of active H* at the Pd surface for the BDE15 debromination (Jadbabaei et al. 2017). Lower solution pH could also prevent ferrous hydroxide from coating on the Pd/Fe nanoparticles surface, which preserved their reactivity (He et al., 2018). However, when the solution pH decreased from 3.0 to 2.2, the BDE15 degradation efficiency decreased to 94.8% within 60 min. It might be due to the excessive hydrogen production from the corrosion of nZVI at strong acidic condition, which agglomerated to the surfaces of Pd/Fe nanoparticles as a barrier (Huang et al. 2018; Sun et al. 2019), hindering the subsequent degradation of BDE15. Moreover, strongly acidic condition could also lead to higher release of the employed Pd (Hildebrand et al. 2009), which was not conducive to the degradation of BDE15 by OP-Pd/Fe. Fig. S2e and Table 1S also indicated that the k_{obs2} value decreased with the increasing solution pH from 3.0 to 11.0. For instance, the k_{obs2} value was 0.0957 min^{-1} when solution pH was 3.0. In contrast, when the solution pH increased to 11.0, the k_{obs2} value decreased to 0.0215 min^{-1}. However, when the solution pH decreased from 3.0 to 2.2, the k_{obs2} value decreased to 0.0577 min^{-1}.

Surprisingly, the degradation efficiencies could also reach 100% and 98.7% after 240 min when the solution initial pH values were 9.0 and 11.0, respectively. The result indicated that the activity of OP-Pd/Fe in the basic pH range was higher than that of many reported nZVI based catalysts (Pang et al. 2014; Liu et al. 2015; Tang et al. 2015; Zhang et al. 2015). Thus, no or less pH adjustment of the medium was required for effective debromination of BDE15 by OP-Pd/Fe over wider pH range, which was conducive to practical application.

In order to further evaluate the catalytic activity of the OP-Pd/Fe, the comparison of degradation activity of some low brominated PBDEs by nZVI/Pd composite with other studies was listed in Table 2S. Huang et al. (2018) uesd polyanionic cellulose stabilized Pd/Fe (Pd loading, 0.3 *wt*%) to degrade BDE47 in Brij35

solution. The degradation efficiency could reach 100% within 15 min, and the rate constant k_{obs} was 18.18 h^{-1}. Wang et al. (2017, 2019) and Lv et al. (2016) also investigated the degradation of BDE47 by nZVI/Pd composite with different Pd loading, the results indicated that the degradation efficiencies were decided by both the Pd loadings and initial BDE47 concentrations. Zhuang et al. (2011) compared the rate constants of five brominated PBDEs by nZVI/Pd under the same conditions and concluded that degradation activities were different for various PBDE congeners, the k_{obs} ranged from 0.066 h^{-1} to 0.126 h^{-1}. In this study, the selected Pd loading of OP-Pd/Fe was only 0.05% wt_{Fe}, and the initial concentration of BDE15 was much higher than that of these previous studies. For example, Wang et al. (2019) studied the degradation of BDE47 (2 mg/L) by 5 g/L nZVI/Pd (Pd loading, 1 *wt*%) and 100% BDE47 was degraded within 60 min, the k_{obs} was 7.05 h^{-1}. However, the degradation efficiency and k_{obs} of BDE15 (10 mg/L) by 3 g/L OP-Pd/Fe (Pd loading, 0.1 *wt*%) was 99.5% and 6.02 h^{-1} within 60 min, respectively. Although, the low PBDE congeners in Table 2S were different, in general, the degradation activity of BDE15 by OP-Pd/Fe was still satisfied compared to previous studies.

Conclusions

The synthesized OP-Pd/Fe exhibited excellent removal capacity to BDE15 under the optimum conditions. Pd loading, catalyst dosage, initial BDE15 concentration, solvent conditions, and pH played significant roles in the removal of BDE15 with OP-Pd/Fe. A two-stage adsorption/debromination removal mechanism was also proposed. During the stage of adsorption, the support OP was an efficient adsorbent for adsorbing BDE15 molecules in solution. In the reductive debromination stage, the Pd/Fe bimetallic nanoparticles efficiently supported by OP worked as an excellent catalyst for degrading BDE15. The removal of BDE15 by OP-Pd/Fe fitted well to the pseudo first-order kinetic equation. The stepwise debromination was the predominant degradation pattern of BDE15, where BDE15 could be completely debrominated to diphenyl ether (DE) under suitable conditions. The results showed a systematic proof-of-principle that efficient debromination was possible with our approach. Therefore, this work implies that OP-Pd/Fe has the potential application in PBDEs elimination. Nevertheless, in the present study, some relevant parameters (e.g. high BDE 15 concentration and THF solvent) do not correspond to relevant environmental conditions, there are still many practical factors to be considered in the future practical application of OP-Pd/Fe.

Declarations

Authors contributions

Jiang Shao, Yi Zhang, and Ziyan Chen performed the experimental work. Zongtang Liu conceptualized, revised the manuscript, and supervised the work. Zhenghao Fei and Yufeng Sun participated in the drafting and revising of the manuscript. Xiaoju Wen, Weizhong Shi, and Dandan Wang participated in data analysis. Chenggang Gu reviewed and revised the manuscript. All authors read and approved the final manuscript.

Funding

This work was supported by the National Natural Science Foundation of China (No.41877118, 41977356, and 21906141), Natural Science Foundation of Jiangsu Province of China (No.BK20181479), Industry-University-Research Cooperation Project of Jiangsu Province (No.BY2020622), Jiangsu Province Undergraduate Innovation and Entrepreneurship training program (202110324008Z), Jiangsu Province Emergency Management Science and Technology Project (YJGL-TG-2020-10), Jiangsu Province Education Department Major Project (No.19KJA140003), Jiangsu Agriculture Science and Technology Innovation Fund (No.CX(20)3169), and sponsored by Qinglan Project of Jiangsu Province of China.

Data availability

The datasets used and/or analyzed during the current study are available from the corresponding author on reasonable request.

Ethics approval Not applicable.

Consent to participate Not applicable.

Consent for publication Not applicable.

Competing interests The authors declare no competing interests.

References

Bohm L, Schlechtriem C, During R (2016) Sorption of highly hydrophobic organic chemicals to organic matter relevant for fish bioconcentration studies. Environ Sci Technol 50(15):8316–8323. https://doi.org/10.1021/acs.est.6b01778

Chen Y, Zhang A, Li H, Peng Y, Lou X, Liu M, Hu J, Liu C, Wei B, Jin J (2020a) Concentrations and distributions of polybrominated diphenyl ethers (PBDEs) in surface soils and tree bark in Inner Mongolia, northern China, and the risks posed to humans. Chemosphere 247:125950. https://doi.org/10.1016/j.chemosphere.2020.125950

Chen Y, Chen T, Liu H, Zhang P, Wang C, Dong S, Chen D, Xie J, Zou X, Suib SL, Li C (2020b) High catalytic performance of the Al-promoted Ni/Palygorskite catalysts for dry reforming of methane. Appl Clay Sci 188:105498. https://doi.org/10.1016/j.clay.2020.105498

Cheng J, Ko FC (2018) Occurrence of PBDEs in surface sediments of metropolitan rivers: Sources, distribution pattern, and risk assessment. Sci Total Environ 637–638:1578–1585. https://doi.org/10.1016/j.scitotenv.2018.05.075

Doong RA, Lai YL (2006) Effect of metal ions and humic acid on the dechlorination of tetrachloroethylene by zerovalent iron. Chemosphere 64:371–378. https://doi:10.1016/j.chemosphere.2005.12.038

Duan J, Zhu H, Xu F, Zhao J (2016) A new approach to 4-chlorophenol dechlorination on monometallic copper compared to its Cu/Fe bimetallic system. Chem Eng J 304:282–288. http://dx.doi.org/10.1016/j.cej.2016.06.089

Ezzatahmadi N, Ayoko GA, Millar GJ, Speight R, Yan C, Li J, Li S, Zhu J, Xi Y (2017). Clay-supported nanoscale zero-valent iron composite materials for the remediation of contaminated aqueous solutions: A review. Chem Eng J 312:336–350. http://dx.doi.org/10.1016/j.cej.2016.11.154

Fang Z, Qiu X, Chen J, Qiu X (2011a) Debromination of polybrominated diphenyl ethers by Ni/Fe bimetallic nanoparticles: influencing factors, kinetics, and mechanism. J Hazard Mater 185:958–969. http://doi:10.1016/j.jhazmat.2010.09.113

Fang Z, Qiu X, Chen J, Qiu X (2011b) Degradation of the polybrominated diphenyl ethers by nanoscale zero-valent metallic particles prepared from steel pickling waste liquor. Desalination 267:34–41. http://doi:10.1016/j.desal.2010.09.003

Guo H, Zhang H, Li Q, Peng F, Xiong L, Wang C, Hu A, Yao S, Chen X (2020) Removal of olefins from reforming aromatic hydrocarbons over metal-halide-modified acid-activated palygorskite. Energ Fuel 34:9463–9472. https://dx.doi.org/10.1021/acs.energyfuels.0c01529

Guo S, Zhu L, Majima T, Lei M, Tang H (2019) Reductive debromination of polybrominated diphenyl ethers: dependence on Br number of the Br-rich phenyl ring. Environ Sci Technol 53 (8):4433–4439. DOI: 10.1021/acs.est.8b07050

He Y, Lin H, Luo M, Liu J, Dong Y, Li B (2020) Highly efficient remediation of groundwater co-contaminated with Cr(VI) and nitrate by using nano-Fe/Pd bimetal-loaded zeolite: Process product and interaction mechanism. Environ Pollut 263:114479. https://doi.org/10.1016/j.envpol.2020.114479

He Y, Lin H, Dong Y, Li B, Wang L, Chu S, Luo M, Liu J (2018) Zeolite supported Fe/Ni bimetallic nanoparticles for simultaneous removal of nitrate and phosphate: Synergistic effect and mechanism. Chem Eng J 347:669–681. https://doi.org/10.1016/j.cej.2018.04.088

Hildebrand H, Mackenzie K, Kopinke FD (2009) Highly active Pd-on-magnetite nanocatalysts for aqueous phase hydrodechlorination reactions. Environ Sci Technol 43:3254–3259. Doi: 10.1021/es802726v

Hou X, Chen X, Bi S, Li K, Zhang C, Wang J, Zhang W (2020) Catalytic degradation of TCE by a PVDF membrane with Pd-coated nanoscale zero-valent iron reductant. Sci Total Environ 702:135030. https://doi.org/10.1016/j.scitotenv.2019.135030

Huang G, Wang M, Hu Y, Cheng J, Lv S, Yang K (2018) Reductive degradation of 2,2',4,4'-tretrabromodiphenyl ether with PAC-Pd/Fe nanoparticles: Effects of Pd loading, initial pH and HA, and degradation pathway. Chem Eng J 334:1252–1259. https://doi.org/10.1016/j.cej.2017.11.077

Huang J, Liu Y, Jin Q, Wang X, Yang J (2007) Adsorption studies of a water soluble dye, Reactive Red MF-3B, using sonication-surfactant-modified attapulgite clay. J Hazard Mater 143:541–548. https://doi:10.1016/j.jhazmat.2006.09.088

Huang Q, Liu W, Peng P, Huang W (2013) Reductive dechlorination of tetrachlorobisphenol A by Pd/Fe bimetallic catalysts. J Hazard Mater 262:634–641. http://dx.doi.org/10.1016/j.jhazmat.2013.09.015

Jadbabaei N, Ye T, Shuai D, Zhang H (2017) Development of palladium-resin composites for catalytic hydrodechlorination of 4-chlorophenol. Appl Catal B-Environ 205:576–586. http://dx.doi.org/10.1016/j.apcatb.2016.12.068

Kim JH, Tratnyek PG, Chang YS (2008) Rapid Dechlorination of polychlorinated dibenzo-p-dioxins by bimetallic and nanosized zerovalent iron. Environ Sci Technol 42:4106–4112. https://doi:10.1021/es702560k

Labunska I, Harrad S, Santillo D, Johnston P, Brigden K (2013) Levels and distribution of polybrominated diphenyl ethers in soil, sediment and dust samples collected from various electronic waste recycling sites within Guiyu town, southern China. Environ Sci: Proc Imp 15:503–511. https://doi:10.1039/c2em30785e

Lei M, Wang Z, Zhu L, Nie W, Tang H (2020) Complete debromination of 2,2',4,4'-tetrabromodiphenyl ether by visible-light photocatalysis on g-C_3N_4 supported Pd. Appl Catal B-Environ 261:118236. https://doi.org/10.1016/j.apcatb.2019.118236

Li H, Zhu F, He S (2019) The degradation of decabromodiphenyl ether in the e-waste site by biochar supported nanoscale zero-valent iron / persulfate. Ecotox Environ Safe 183:109540. https://doi.org/10.1016/j.ecoenv.2019.109540

Li R, Jin X, Megharaj M, Naidu R, Chen Z (2015) Heterogeneous Fenton oxidation of 2,4-dichlorophenol using iron-based nanoparticles and persulfate system. Chem Eng J 264:587–594. http://dx.doi.org/10.1016/j.cej.2014.11.128

Liu Z, Zhang G, Wang MK (2014) Immobilization of polychlorinated biphenyls in contaminated soils using organoclays. Appl Clay Sci 101:297–303. http://dx.doi.org/10.1016/j.clay.2014.08.018

Liu Z, Gu C, Ye M, Bian Y, Cheng Y, Wang F, Yang X, Song Y, Jiang X (2015) Debromination of polybrominated diphenyl ethers by attapulgite-supported Fe/Ni bimetallic nanoparticles: Influencing factors, kinetics and mechanism. J Hazard Mater 298:328–337. http://dx.doi.org/10.1016/j.jhazmat.2015.05.032

Lv Y, Zhang Z, Chen Y, Hu Y (2016) A novel three-stage hybrid nano bimetallic reduction/oxidation/biodegradation treatment for remediation of 2,2',4,4'-tetrabromodiphenyl ether. Chem Eng J 289:382–390. http://dx.doi.org/10.1016/j.cej.2015.12.097

Mokete R, Eljamal O, Sugihara Y (2020) Exploration of the reactivity of nanoscale zero-valent iron (NZVI) associated nanoparticles in diverse experimental conditions. Chem Eng Process 150:107879. https://doi.org/10.1016/j.cep.2020.107879

Muresan B, Lorgeoux C, Gasperi J, Moilleron R (2010) Fate and spatial variations of polybrominated diphenyl ethers in the deposition within a heavily urbanized area: case of Paris (France). Water Sci Technol 62:822–828. https://doi:10.2166/wst.2010.931

Ni H, Ding C, Lu S, Yin X, Samuel SO (2012) Food as a main route of adult exposure to PBDEs in Shenzhen, China. Sci Total Environ 437:10–14. http://dx.doi.org/10.1016/j.scitotenv.2012.07.056

Pang Z, Yan M, Jia X, Wang Z, Chen J (2014) Debromination of decabromodiphenyl ether by organo-montmorillonite-supported nanoscale zero-valent iron: Preparation, characterization and influence factors. J Environ Sci 26:483–491. https://doi:10.1016/S1001-0742(13)60419-2

Qin P, Ni H, Liu Y, Shi Y, Zeng H (2011) Occurrence, distribution, and source of polybrominated diphenyl ethers in soil and leaves from Shenzhen Special Economic Zone, China. Environ Monit Assess 174:259–270. https://doi:10.1007/s10661-010-1455-y

Sarkar D, Singh SK (2021) Decabromodiphenyl ether (BDE-209) exposure to lactating mice perturbs steroidogenesis and spermatogenesis in adult male offspring. Ecotox Environ Safe 209:111783. https://doi.org/10.1016/j.ecoenv.2020.111783

Shen W, Mu Y, Wang B, Ai Z, Zhang L (2017) Enhanced aerobic degradation of 4-chlorophenol with iron-nickel nanoparticles. Appl Surf Sci 393:316–324. http://dx.doi.org/10.1016/j.apsusc.2016.10.020

Smuleac V, Varma R, Sikdar S, Bhattacharyya D (2011) Green synthesis of Fe and Fe/Pd bimetallic nanoparticles in membranes for reductive degradation of chlorinated organics. J Membrane Sci 379:131–137. http://doi:10.1016/j.memsci.2011.05.054

Sun Y, Liu Z, Fei Z, Li C, Chun Y, Zhang A (2019) Synergistic effect and degradation mechanism on Fe-Ni/CNTs for removal of 2,4-dichlorophenol in aqueous solution. Environ Sci Pollut Res 26:8768–8778. https://doi.org/10.1007/s11356-019-04394-w

Talpade AD, Tiwari MS, Yadav GD (2019) Selective hydrogenation of bio-based 5-hydroxymethyl furfural to 2,5-dimethylfuran over magnetically separable Fe-Pd/C bimetallic nanocatalyst. Mol Catal 465:1–15. https://doi.org/10.1016/j.mcat.2018.12.009

Tan L, Lu S, Fang Z, Cheng W, Tsang EP (2017) Enhanced reductive debromination and subsequent oxidative ring-opening of decabromodiphenyl ether by integrated catalyst of nZVI supported on magnetic Fe_3O_4 nanoparticles. Appl Catal B-Environ 200:200–210. http://dx.doi.org/10.1016/j.apcatb.2016.07.005

Tang L, Tang J, Zeng G, Yang G, Xie X, Zhou Y, Pang Y, Fang Y, Wang J, Xiong W (2015) Rapid reductive degradation of aqueous p-nitrophenol using nanoscale zero-valent iron particles immobilized on mesoporous silica with enhanced antioxidation effect. Appl Surf Sci 333:220–228. http://dx.doi.org/10.1016/j.apsusc.2015.02.025

Wang F, Gao Y, Sun Q, Chen Z, Megharaj M, Naidu R (2014) Degradation of microcystin-LR using functional clay supported bimetallic Fe/Pd nanoparticles based on adsorption and reduction. Chem Eng J 255:55–62. http://dx.doi.org/10.1016/j.cej.2014.06.003

Wang R, Lu G, Lin H, Huang K, Tang T, Xue X, Yang X, Yin H, Dang Z (2017) Relative roles of H-atom transfer and electron transfer in the debromination of polybrominated diphenyl ethers by palladized nanoscale zerovalent iron. Environ Pollut 222:331–337. http://dx.doi.org/10.1016/j.envpol.2016.12.030

Wang R, Tang T, Lu G, Zheng Z, Huang K, Li H, Tao X, Yin H, Shi Z, Lin Z, Wu F, Dang Z (2019) Mechanisms and pathways of debromination of polybrominated diphenyl ethers (PBDEs) in various nano-zerovalent iron-based bimetallic systems. Sci Total Environ 661:18–26. https://doi.org/10.1016/j.scitotenv.2019.01.166

Wang X, Yang J, Zhu M, Li F (2013) Characterization and regeneration of Pd/Fe nanoparticles immobilized in modified PVDF membrane. J Taiwan Inst Chem E 44:386–392. http://dx.doi.org/10.1016/j.jtice.2012.12.007

Wang Y, Zhou D, Wang Y, Zhu X, Jin S (2011) Humic acid and metal ions accelerating the dechlorination of 4-chlorobiphenyl by nanoscale zero-valent iron. J Environ Sci 23:1286–1292. https://doi:10.1016/S1001-0742(10)60543-8

Wei L, Zhou B, Xiao K, Yang B, Yu G, Li J, Zhu C, Zhang J, Duan H (2020a) Highly efficient degradation of 2,2',4,4'-tetrabromodiphenyl ether through combining surfactant-assisted Zn^0 reduction with subsequent Fenton oxidation. J Hazard Mater 385:121551. https://doi.org/10.1016/j.jhazmat.2019.121551

Wei X, Zhu N, Huang X, Kang N, Wu P, Dang Z (2020b) Efficient degradation of sodium diclofenac via heterogeneous Fenton reaction boosted by Pd/Fe@Fe_3O_4 nanoparticles derived from bio-recovered palladium. J Environ Manage. 260:110072. https://doi.org/10.1016/j.jenvman.2020.110072

Weng X, Chen Z, Chen Z, Megharaj M, Naidu R (2014a) Clay supported bimetallic Fe/Ni nanoparticles used for reductive degradation of amoxicillin in aqueous solution: Characterization and kinetics. Colloid Surface A 443:404–409. http://dx.doi.org/10.1016/j.colsurfa.2013.11.047

Weng X, Sun Q, Lin S, Chen Z, Megharaj M, Naidu R (2014b) Enhancement of catalytic degradation of amoxicillin in aqueous solution using clay supported bimetallic Fe/Ni nanoparticles. Chemosphere 103:80–85. http://dx.doi.org/10.1016/j.chemosphere.2013.11.033

Wiltschka K, Neumann L, Werheid M, Bunge M, During R, Mackenzie K, Bohm L (2020) Hydrodechlorination of hexachlorobenzene in a miniaturized nano-Pd(0) reaction system combined with the simultaneous extraction of all dechlorination products. Appl Catal B-Environ 275:119100. https://doi.org/10.1016/j.apcatb.2020.119100

Wong F, Kurt-Karakus P, Bidleman TF (2012) Fate of brominated flame retardants and organochlorine pesticides in urban soil: volatility and degradation. Environ Sci Technol 46:2668–2674. http://dx.doi.org/10.1021/es203287x

Wu P, Liu C, Huang Z, Wang W (2014) Enhanced dechlorination performance of 2,4-dichlorophenol by vermiculite supported iron nanoparticles doped with palladium. RSC Adv 4:25580. http://doi:10.1039/c4ra02618g

Wurl O, Lam PK, Obbard JP (2006) Occurrence and distribution of polybrominated diphenyl ethers (PBDEs) in the dissolved and suspended phases of the sea-surface microlayer and seawater in Hong Kong, China. Chemosphere 65:1660–1666. http://doi:10.1016/j.chemosphere.2006.02.024

Xian J, Ma H, Li Z, Ding C, Liu Y, Yang J, Cui F (2021) *a*-FeOOH nanowires loaded on carbon paper anodes improve the performance of microbial fuel cells. Chemosphere 273:129669. https://doi.org/10.1016/j.chemosphere.2021.129669

Xie J, Lei C, Chen W, Xie Q, Guo Q, Huang B (2021) Catalytic properties of transition metals modified nanoscale zero-valent iron for simultaneous removal of 4-chlorophenol and Cr(VI): Efficacy, descriptor and reductive mechanisms. J Hazard Mater 403:123827. https://doi.org/10.1016/j.jhazmat.2020.123827

Xie Y, Fang Z, Qiu X, Tsang E, Liang B (2014) Comparisons of the reactivity, reusability and stability of four different zero-valent iron-based nanoparticles. Chemosphere 108:433–436. http://dx.doi.org/10.1016/j.chemosphere.2014.01.076

Xu J, Sheng T, Hu Y, Baig S, Lv X, Xu X (2013a) Adsorption–dechlorination of 2,4-dichlorophenol using two specified MWCNTs-stabilized Pd/Fe nanocomposites. Chem Eng J 219:162–173. http://dx.doi.org/10.1016/j.cej.2013.01.010

Xu J, Tang J, Baig SA, Lv X, Xu X (2013b) Enhanced dechlorination of 2,4-dichlorophenol by Pd/Fe-Fe_3O_4 nanocomposites. J Hazard Mater 244-245:628–636. http://dx.doi.org/10.1016/j.jhazmat.2012.10.051

Xu Y, Liang C, Zhang T, Tao X, Wang R, Huang K, Pan Z, Dang Z, Yin H, Lu G (2020) Debromination of polybrominated diphenyl ethers (PBDEs) by palladized zerovalent zinc particles: Influence factors, pathways and mechanism. Chemosphere 253:126726. https://doi.org/10.1016/j.chemosphere.2020.126726

Zahran EM, Bhattacharyya D, Bachas LG (2013) Reactivity of Pd/Fe bimetallic nanotubes in dechlorination of coplanar polychlorinated biphenyls. Chemosphere 91:165–171.

http://dx.doi.org/10.1016/j.chemosphere.2012.12.037

Zhang Q, Guo Y, Huang M, Li H, Gu C (2015) Degradation of selected polychlorinated biphenyls by montmorillonite clay-templated Fe^0/Ni^0 bimetallic system. Chem Eng J 276:122–129. http://dx.doi.org/10.1016/j.cej.2015.04.044

Zhou H, Xiang J, Zhao Y, Chen Y (2018) Improvements of Pd/Fe nanoparticles by ethylenediamine disuccinic acid for 2,4-D dechlorination. Sep Purif Technol 207:377–386. https://doi.org/10.1016/j.seppur.2018.06.061

Zhu H, Wang Y, Tam NFY (2014) Microcosm study on fate of polybrominated diphenyl ethers (PBDEs) in contaminated mangrove sediment. J Hazard Mater 265:61–68. http://dx.doi.org/10.1016/j.jhazmat.2013.11.046

Zhuang Y, Ahn S, Luthy RG (2010) Debromination of polybrominated diphenyl ethers by nanoscale zerovalent iron: Pathways, kinetics, and reactivity. Environ Sci Technol 44:8236–8242. http://doi:10.1021/es101601s

Zhuang Y, Ahn S, Seyfferth AL, Masue-Slowey Y, Fendorf S, Luthy RG (2011) Dehalogenation of polybrominated diphenyl ethers and polychlorinated biphenyl by bimetallic, impregnated, and nanoscale zerovalent iron. Environ Sci Technol 45:4896–903. http://dx.doi.org/10.1021/es104312h

Figures

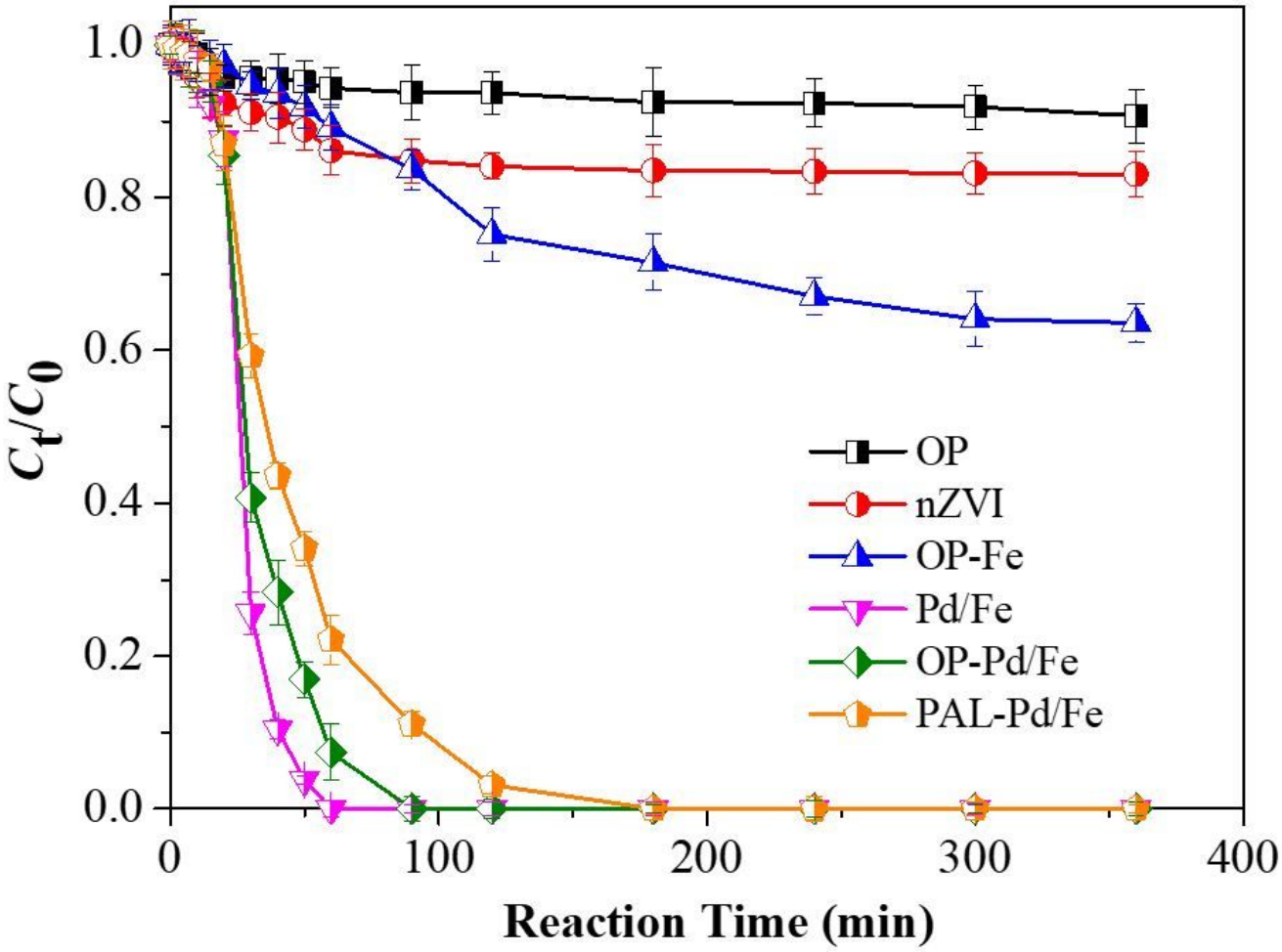

Figure 1

Comparison of BDE15 removal using various material. (Conditions: initial BDE15 concentration, 10 mg/L; Pd loading, 0.05% wtFe; solvent condition, THF/W = 50/50; pH= 7.0; dosages of OP, OP-Fe, OP-Pd/Fe, and PAL-Pd/Fe, 3.0 g/L; dosages of nZVI and Pd/Fe, 1.0 g/L.)

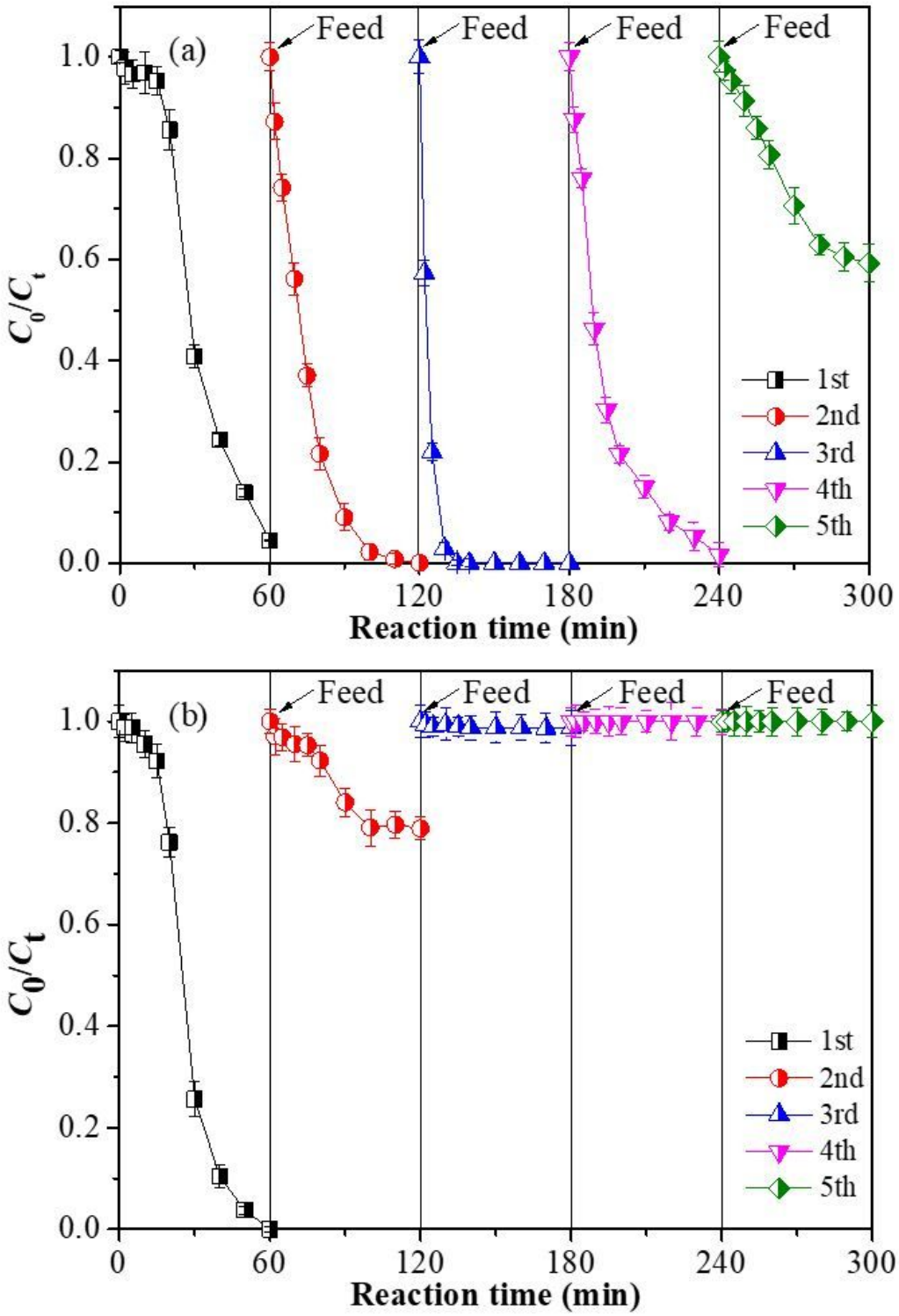

Figure 2

The stability test of (a) OP-Pd/Fe and (b) Pd/Fe (Conditions: initial BDE15 concentration, 10 mg/L; Pd loading, 0.05% wtFe; solvent condition, THF/W = 50/50; pH= 7.0.)

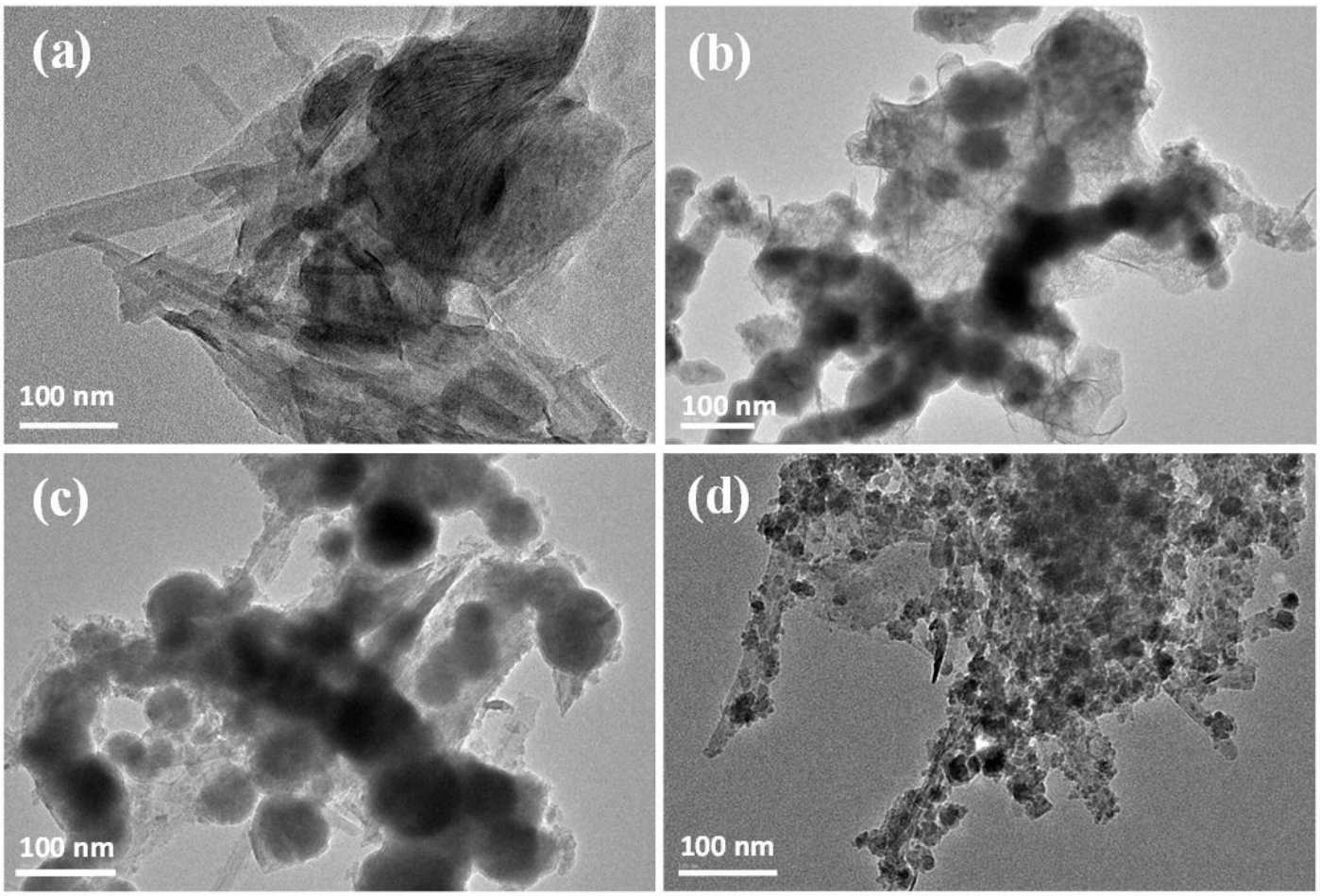

Figure 3

TEM image of (a) OP, (b) Pd/Fe, (c) OP-Pd/Fe (before reaction), and (d) OP-Pd/Fe (after reaction)

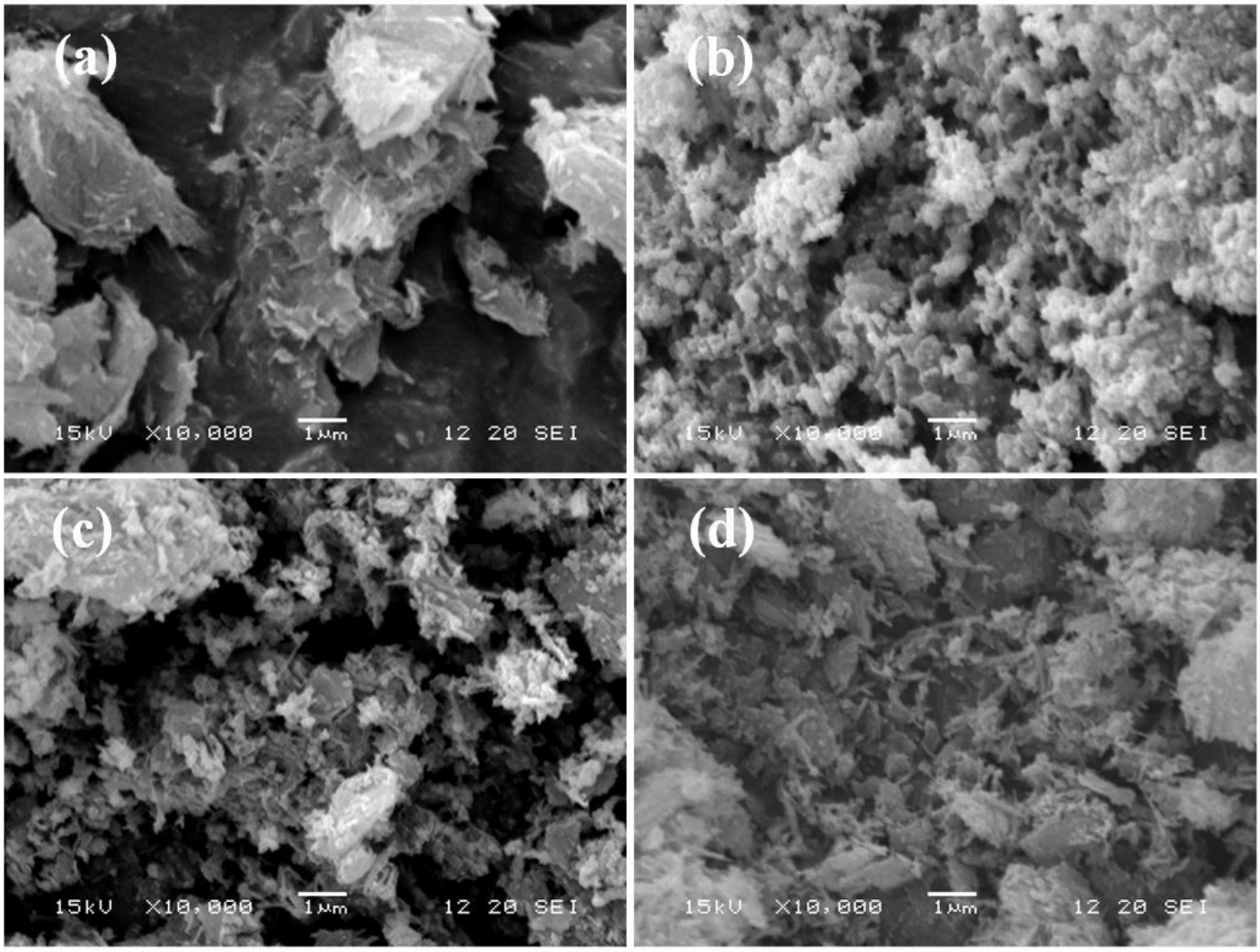

Figure 4

SEM image of (a) OP, (b) Pd/Fe, (c) OP-Pd/Fe (before reaction), and (d) OP-Pd/Fe (after reaction)

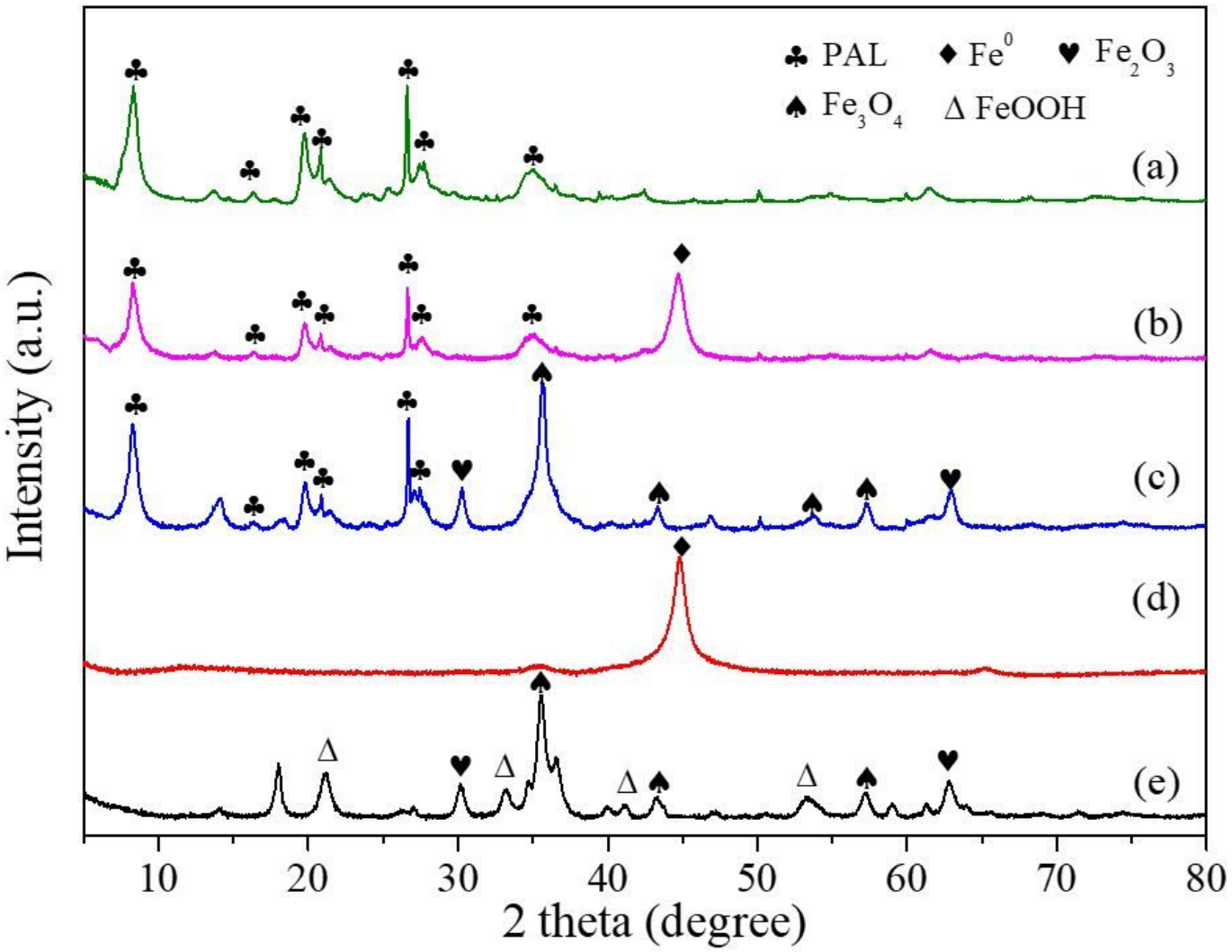

Figure 5

XRD patterns of (a) OP, (b) OP-Pd/Fe (before reaction), (c) OP-Pd/Fe (after reaction), (d) Pd/Fe (before reaction), and (e) Pd/Fe (after reaction)

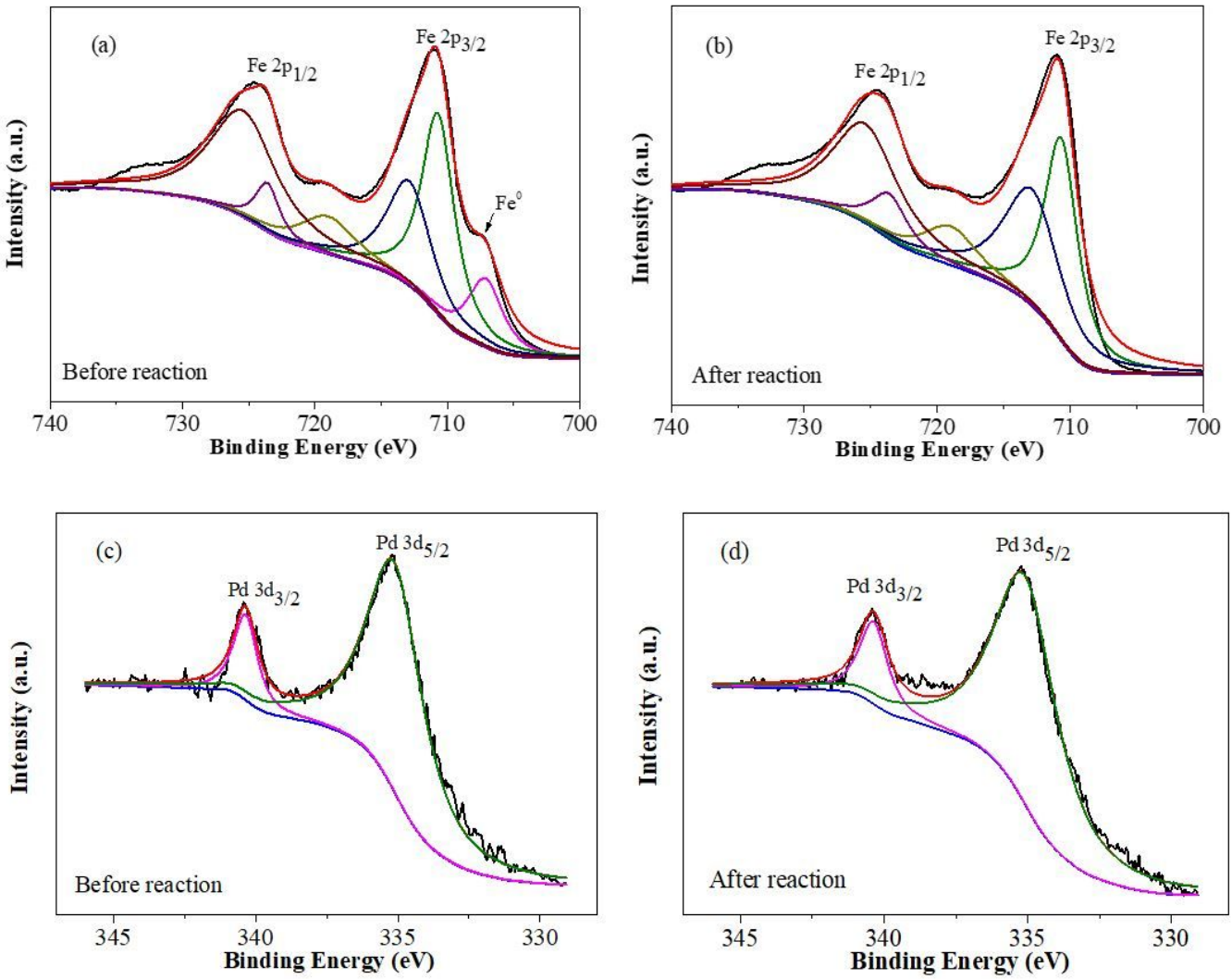

Figure 6

XPS spectra for Fe 2p of (a) OP-Pd/Fe (before reaction) and (b) OP-Pd/Fe (after reaction); XPS spectra for Pd 3d of (c) OP-Pd/Fe (before reaction) and (d) OP-Pd/Fe (after reaction)

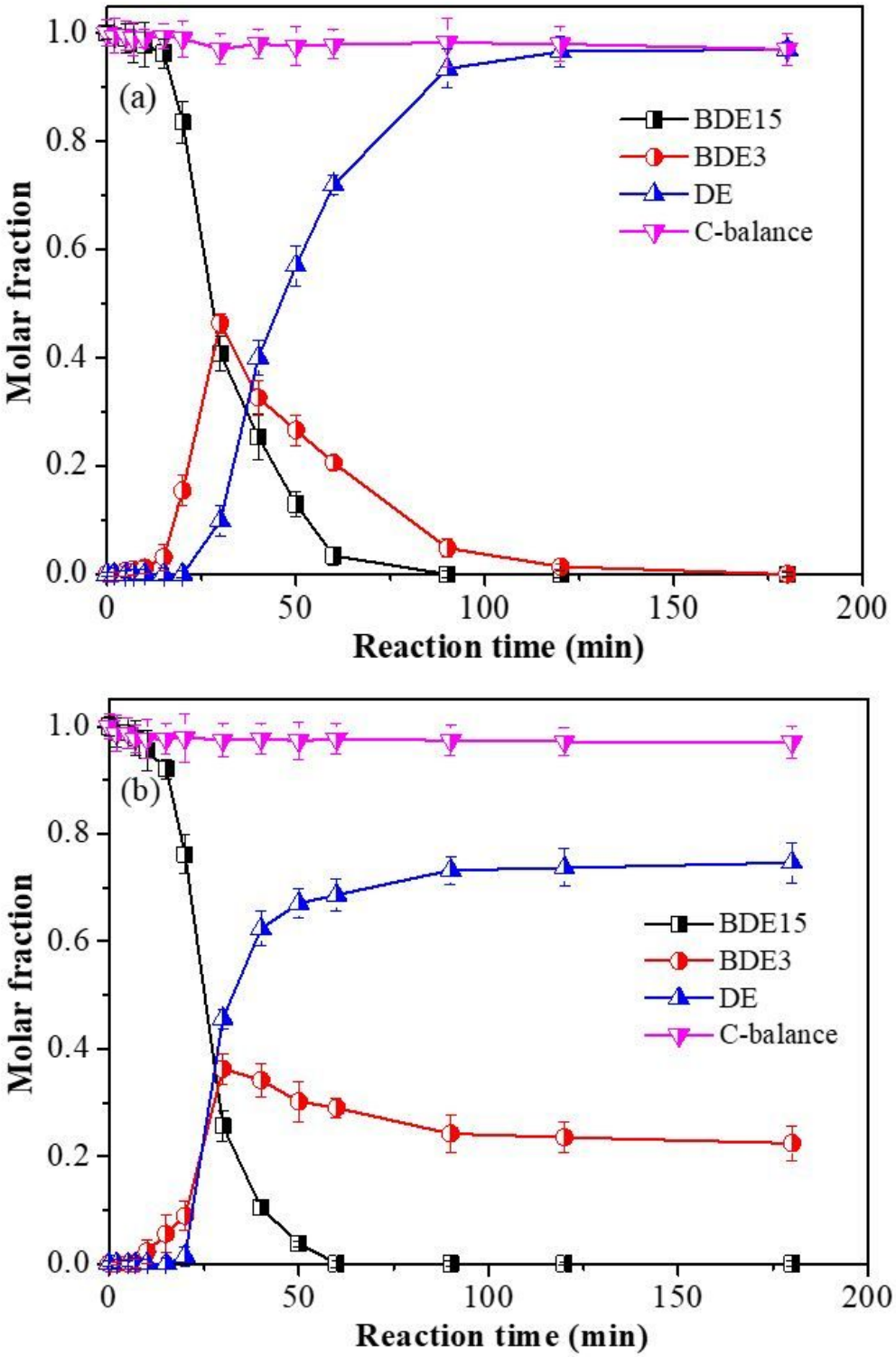

Figure 7

The debromination products of BDE15 by (a) OP-Pd/Fe and (b) Pd/Fe (Conditions: material dosage, 3.0 g/L; Pd loading, 0.05% wtFe; initial BDE15 concentration, 10 mg/L; solvent condition, THF/W = 50/50; pH = 7.0.)

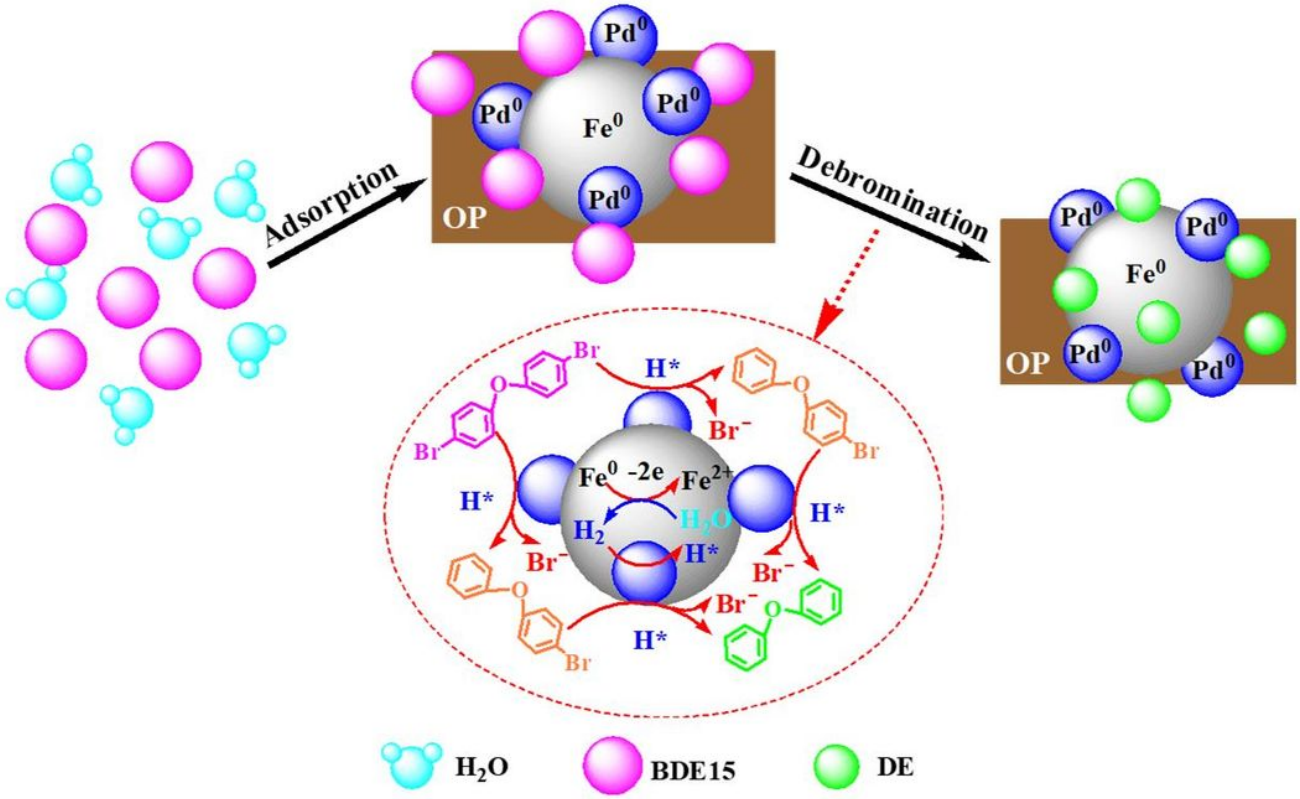

Figure 8

Schematic diagram of removal mechanism between OP-Pd/Fe and BDE15

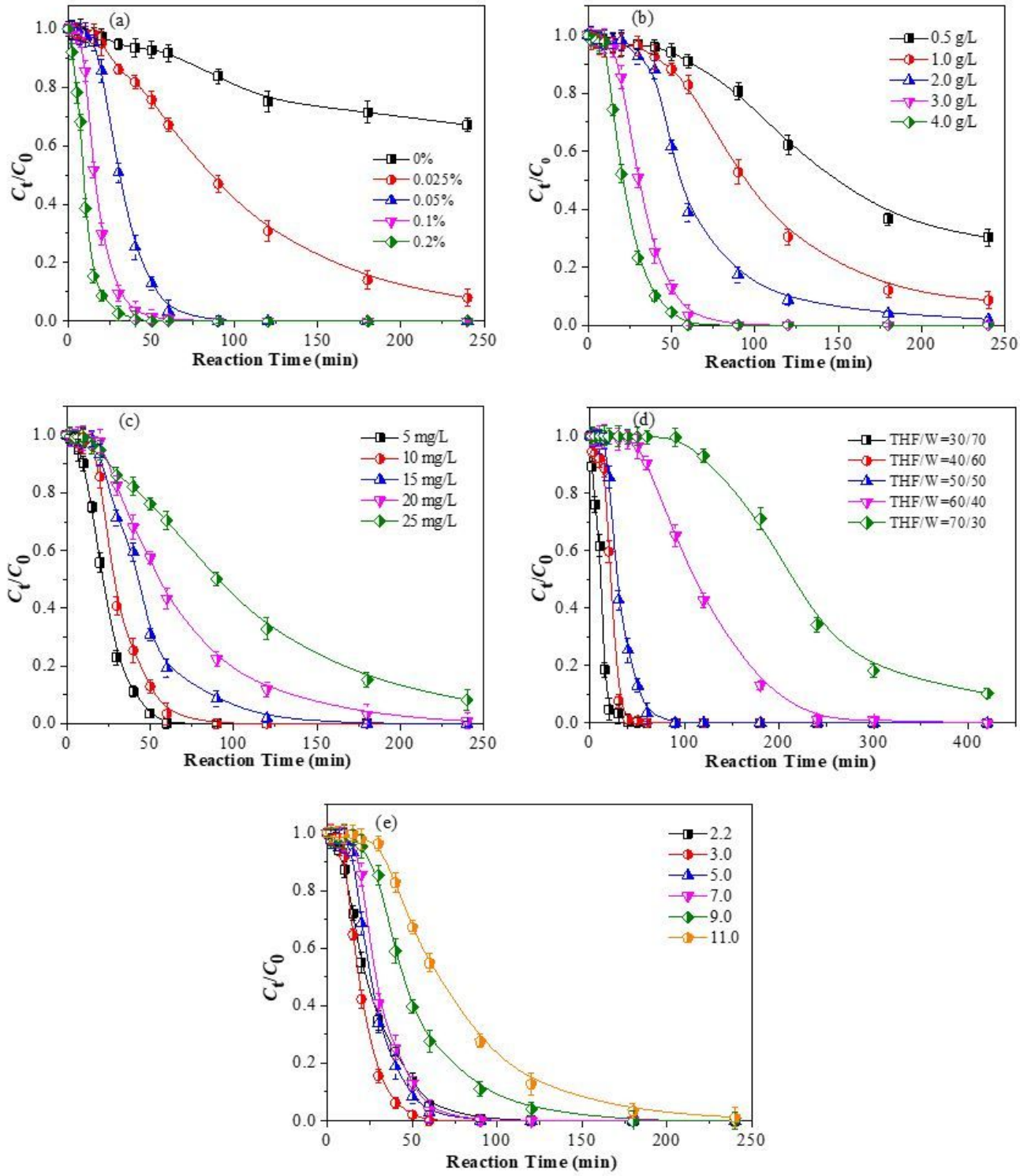

Figure 9

Effect of experimental parameters on the degradation of BDE15: (a) Pd loading; (b) OP-Pd/Fe dosage; (c) initial BDE15 concentration; (d) solvent conditions; (e) pH (Except for the investigated parameter, other parameters fixed on Pd loading 0.05% wtFe, 3.0 g/L OP-Pd/Fe, 10 mg/L BDE15, THF/W = 50/50, and pH = 7.0.)

Supplementary Files

This is a list of supplementary files associated with this preprint. Click to download.

- SupplementaryMaterial.doc